Machine Learning and Image Processing to Monitor Strain and Tensile Forces with Mechanochromic Sensors

Lucas Daniel Chiba de Castro[1], Leonardo Felipe dos Santos Scabini[1], Lucas Correia Ribas[1,2], Odemir Martinez Bruno[1] and Osvaldo Novais de Oliveira Junior[*,1]

[1]São Carlos Institute of Physics, University of São Paulo, 13566-590 São Carlos, SP, Brazil

[2]Institute of Biosciences, Humanities and Exact Sciences, São Paulo State University, 15054-000 São José do Rio Preto, SP, Brazil

**Corresponding author*

E-mail addresses: lucas.castro@ifsc.usp.br (Lucas D. C. de Castro), scabini@ifsc.usp.br (Leonardo F. S. Scabini), lucas.ribas@unesp.br (Lucas C. Ribas), bruno@ifsc.usp.br (Odemir M. Bruno), chu@ifsc.usp.br (Osvaldo N. Oliveira Jr.)

Abstract

A computer vision (CV) system is proposed for real-time prediction of strain by monitoring the color-changing feature of mechanochromic sensors. Pictures of the sensors subjected to calibration tensile tests were treated with standard image processing methods and analyzed using supervised machine learning (ML) algorithms. Visual strain sensing was demonstrated by linear regression models capable of learning a relation between the applied strain and the reflected structural color. The ElasticNet regression model provided the highest accuracy in the strain prediction task, with a remarkable performance in monitoring real-time strain variation of sensors during a tensile-relaxion cycle. Using calibration curves, the predicted strain can also be employed for estimating the tensile force applied on the mechanochromic sensors. Taken together these results point to potential intelligent systems for noninvasive *in-situ* visual monitoring of deformations and tensions.

Keywords: sensors; mechanochromic; computer vision; machine learning; image processing

1. Introduction

Computer vision (CV) and image processing has enabled computers to perceive visual stimuli at a low-cost and noninvasive manner through pictures and videos acquired by digital cameras. This type of machine perception allows for performing simple tasks such as identifying objects and more involved analysis of complex environments (Esteva et al., 2021; Liu et al., 2021; Yuan et al., 2021). Also, CV expands the traditional human-computer interaction (HCI) limited to electronic inputs to a more natural way of connection through visual signals(Ramadoss et al., 2021). Today, flexible and stretchable strain sensors are used in personal health monitoring(Jing Chen et al., 2020; Huang et al., 2021; W. Li et al., 2021; Jilong Wang, Lu, & Zhang, 2020), electronic skins(Z. Gao et al., 2020; Yang et al., 2019; Zhang, Chen, Wang, & Zhao, 2020), soft

robotics(Karipoth, Christou, Pullanchiyodan, & Dahiya, 2022; Lin et al., 2021; Jiangxin Wang, Gao, & Lee, 2021) and human-machine interaction systems(Tian et al., 2019; L. Wang, Liu, Yan, Wang, & Wang, 2021; W. Wang et al., 2021; Yin, Wang, Zhao, Lou, & Shen, 2021; Zhong et al., 2019). Strain sensors convert deformation stimuli into measurable electrical signals (i.e., resistance and/or capacitance)(W. Gao, Ota, Kiriya, Takei, & Javey, 2019; C. Wang et al., 2019; W. Wu, 2019), whose main limitation is the requirement of a power source and connection to external instruments for signal processing and data acquisition(Y. Lee et al., 2020). Obviously, electrical signals cannot be visualized with human eyes, restricting their applications in visual intelligent HCI. In this context, the replacement of electrical signals for a visible output might be an attractive opportunity(Zhao et al., 2021). Using nature as a source of inspiration, colors enable interaction and communication between living organisms in biological and artificial environments. In contrast to regular man-made devices that remain predominantly rigid and energy intensive, some species have developed efficient intracellular structures to change color dynamically in soft tissues with minimal power input(Poloni, Rafsanjani, Place, Ferretti, & Studart, 2022). In some of these animals, structural colors arise from the light interaction with periodically ordered nanostructures known as photonic crystals (PCs). A famous example is the rapid skin color change in chameleons through the active control of the lattice spacing of guanine nanocrystal arrays within cells referred to as iridophores(Teyssier, Saenko, van der Marel, & Milinkovitch, 2015).

Inspired on the chameleon skins, mechanochromic PC-based materials have been used in visual strain sensing because they can provide instantaneous and intuitive visual response(Hu, Wei, Yang, Ma, & Huang, 2022; Kim, Lee, Kim, & Kim, 2020; G. H. Lee et al., 2019; Yi et al., 2019). These materials are normally manufactured by embedding colloidal PCs in soft matrices such as polymer elastomers(Cheng et al., 2020; Hsieh, Lu, & Yang, 2020; M. Li et al., 2020) or hydrogels(Jiayao Chen et al., 2019; Dong et al., 2019; Y. Wang et al., 2021; Y. Wu, Wang, Zhang, & Wu, 2021). Mechanochromic PC-based strain sensors are interesting for their unfading colorimetric signals that are readable without requiring any equipment or external power sources(Qin, Li, & Song, 2022). With a combination of Poisson's effect and Bragg's law, mechanical deformation modifies the PC lattice spacing and changes the apparent reflected color. The color shift is proportional to the elongation ratio and, as the strain (ε) increases, the peak of reflected spectrum (λ_{MAX}) blueshifts along the visible range. This unique relation can be explored for quantifying strain, especially with efficient mechanochromic devices(C de Castro & Oliveira, 2022). The sensors in the latter reference are near-perfect elastic and exhibit reversible structural color change under stretching/releasing cycles. They are nevertheless limited to convert mechanical stimuli into color changing response. In other words, quantifying a strain input based on visual perception of the reflected color would be impossible even for a trained person. Furthermore, since the blueshift of λ_{MAX} is proportional to ε, small deformations induce only slight color changes that might not be perceived with naked eyes and could go unnoticed for a human observer.

In this work we propose a new metaphor for replacing human observers by a CV system for predicting mechanical deformation based on the reflected structural color of the mechanochromic devices above**.** As a proof-of-concept, we developed a machine learning pipeline to monitor strain-induced color-changing mechanisms and predict the applied strain in real-time, which can also be used for estimating the tensile force. The machine learning algorithm was trained with traditional models of linear regression that can be continuously updated through acquisition of new digital images. Even though the algorithm was trained with a static image constrained to discrete integer classes, it learned a linear relation between λ_{MAX} and ε, being able to infer any real-valued strain within the analyzed range. The CV system enables a continuous and automated monitoring of strain and tensile forces in an *in-situ*, flexible and noninvasive manner with remarkable accuracy.

2. Materials and methods

2.1. Preparation of the photonic ink

Nearly monodisperse silica nanoparticles (SiO_2, d = 185nm, PDI = 0.009) were synthesized via Stöber process (Stöber, Fink, & Bohn, 1968) and dispersed in ethanol. The homogeneous SiO_2 suspension was mixed with poly(ethylene glycol) phenyl ether acrylate (PEGPEA, Mn ~ 324, Sigma-Aldrich) containing 1 wt.% of 2-hydroxy-2-methylpropiophenone (97%, Sigma-Aldrich) in a volume ratio of 0.35, considering an ethanol-free basis. After complete evaporation of ethanol in an oven, a colloidal photocurable photonic ink was obtained.

2.2. Fabrication of the mechanochromic strain sensors

Briefly, a droplet of the photonic ink was molded in between two microscope glass slides and irradiated with UV-light to prepare the mechanoresponsive core. The core was encapsulated by two layers of poly(dimethylsiloxane) (PDMS, Sylgard 184, Dow Corning), a pristine PDMS (transparent) and a black PDMS (dyed with 2 wt.% of carbon black), both containing 10 wt.% of cross-linker. After successive degassing and thermal curing steps, the mechanochromic strain sensor was obtained. The detailed protocol to manufacture mechanochromic devices with multilayered architecture has been reported in the literature (C de Castro & Oliveira, 2022).

2.3. Sensing measurements and image acquisition

Sensing measurements of the mechanochromic devices were performed in a universal testing machine (Instron 5969), operating in tensile mode under controlled strain (ε). A set of five individual specimens were tested in three replicates. Prior to the measurements, stress/relaxation precycling was imposed to minimize macromolecular relaxation interferences. The strain-controlled tensile tests were conducted in isolated runs with consecutive increasing steps of ε = 2%, starting from 0% until 20%. In each discreet strain level, pictures of the sensors were taken with an ordinary digital camera (Nikon D5300) set in AUTO mode. The described procedure

resulted in a total of 165 images manually labeled according to each discrete strain level ∈ {0, 2, 4, 6, 8, 10, 12, 14, 16, 18, 20}.

2.4. Image preprocessing

Prior to the training stage of the Machine Learning model, the pictures of the devices were converted from the standard RGB to the HSV color-space and preprocessed. For this, we applied an empirically defined thresholding in the HSV ranges [85, 135]; [0, 255]; [0, 255]. The resulting HSV representation was converted to grayscale by pixel average and a binary thresholding was applied in the range [50, 255] to isolate the mechanochromic core from the background pixels. To further improve the segmented region, the following sequence of morphological operations was performed: an erosion with a 7 x 7 kernel, a dilation with a 3 x 3 kernel, another erosion with a 3 x 3 kernel followed by a final dilation with a 3 x 3 kernel. These techniques are a standard part of image analysis toolbox as referred elsewhere (Dougherty & Lotufo, 2003).

2.5. Training and validating the ML model

After the preprocessing steps, the dataset consists of items from isolated regions of each image of the mechanochromic sensor obtained after segmentation. In this sense, each data point represents the region of a single image of the mechanochromic sensor. We then characterized this region by computing the frequency of pixel intensity in each channel (with sizes 255, 255, and 180 for H, S, and V, respectively) and combining them into a single image descriptor (HSV descriptor of size 690). These descriptors are the input training vectors for the ML models. The dataset of preprocessed pictures was split into training and test sets in a 5-fold cross validation strategy. 5 equally-sized and equally-distributed groups were randomly created, in which 4 were used for training the model and 1 was used for testing. Five repetitions were needed to evaluate the model on each fold while training it on the other 4 remaining folds. The whole process was repeated 10 times and the result was measured among 50 trials (10 repetitions of 5-fold cross validation). We also considered a more realistic validation approach where all samples of a single sensor were used for training the model, while the remaining sensors were used for testing. Hence, we evaluated how the model reacts to newly produced sensors that it did not see during the training step (sensor-wise validation). The results were expressed as the coefficient of determination of the prediction (R^2), calculated as the fraction between the sum of squares of residuals and the total sum of squares, given the *ground truth* obtained from the controller software of the tensile machine and the *predicted strain* by our algorithm in each picture.

2.6. Testing the CV system in real-time strain prediction

The real-time strain prediction of the algorithm was evaluated with the aid of a universal testing machine (Instron 5969), operating in tensile mode under controlled ε. A video of each individual specimen was recorded during a tensile test conducted as follows: stretching from ε = 0% to 20%;

followed by a lapse of 5 s and releasing from ε = 20% to 0%. To be consistent with the training step, the tensile tests were recorded with an ordinary digital camera (Nikon D5300) set in AUTO mode and the algorithm's prediction was compared to the real strain values obtained from the controller software of the equipment.

2.7. Estimation of theoretical tensile forces applied on the sensors

A linear function was fitted on the strain-load curve obtained from the controller software of the tensile machine. The theoretical tensile forces applied on the sensors were estimated by inputting the predicted strain values on this function and compared to the real data.

3. Results and discussion

The sensors are prepared by encapsulating a mechanochromic core in-between a pristine and a black PDMS layer. This multilayered architecture ensures mechanical robustness and high saturated structural colors, allowing the devices to detect deformations on real time through a visual output. The mechanoresponsive core consists of a self-assembled SiO_2 face-centered-cubic (FCC) structure embedded in a photopolymerized PEGPEA supersaturated suspension (**Figure 1a**). The detection principle is based on a combination of Bragg's law and Poisson's effect as a PC array can be modulated via mechanical deformation of their architecture, with the ensuing change in apparent structural color. When light irradiates the mechanochromic material at normal incidence, the peak of reflected spectrum (λ_{MAX},) will appear at a set of wavelengths according to **Eq. 1:**

$$\lambda_{MAX} = 2d_{(111)}n_{eff}(1 - \nu\varepsilon) \qquad \textbf{Eq. 1}$$

where $d_{(111)}$ is the interlayer lattice spacing, n_{eff} is the effective refractive index, ν is the Poisson's ratio, and ε is the elongation ratio along the longitudinal direction(Hsieh et al., 2020). Assuming a constant n_{eff} and a perfect elastic behavior, stretching reduces the thickness and $d_{(111)}$, and thereby blueshifts the reflected spectrum. The apparent structural color is dictated by the applied strain and is discrete for each ε value (**Figure 1b-c**)(Hu, Yang, Ma, & Huang, 2022; G. H. Lee et al., 2017). The devices used here exhibit a near-perfect elastic behavior at low strain values but are still limited to convert mechanical stimuli into eye-perceptible color changes (**Figure 1d-e**). Nonetheless, we believe that the unique relation between λ_{MAX} and ε might be explored for strain quantification through visual sensing with the CV system depicted in **Figure 1f**.

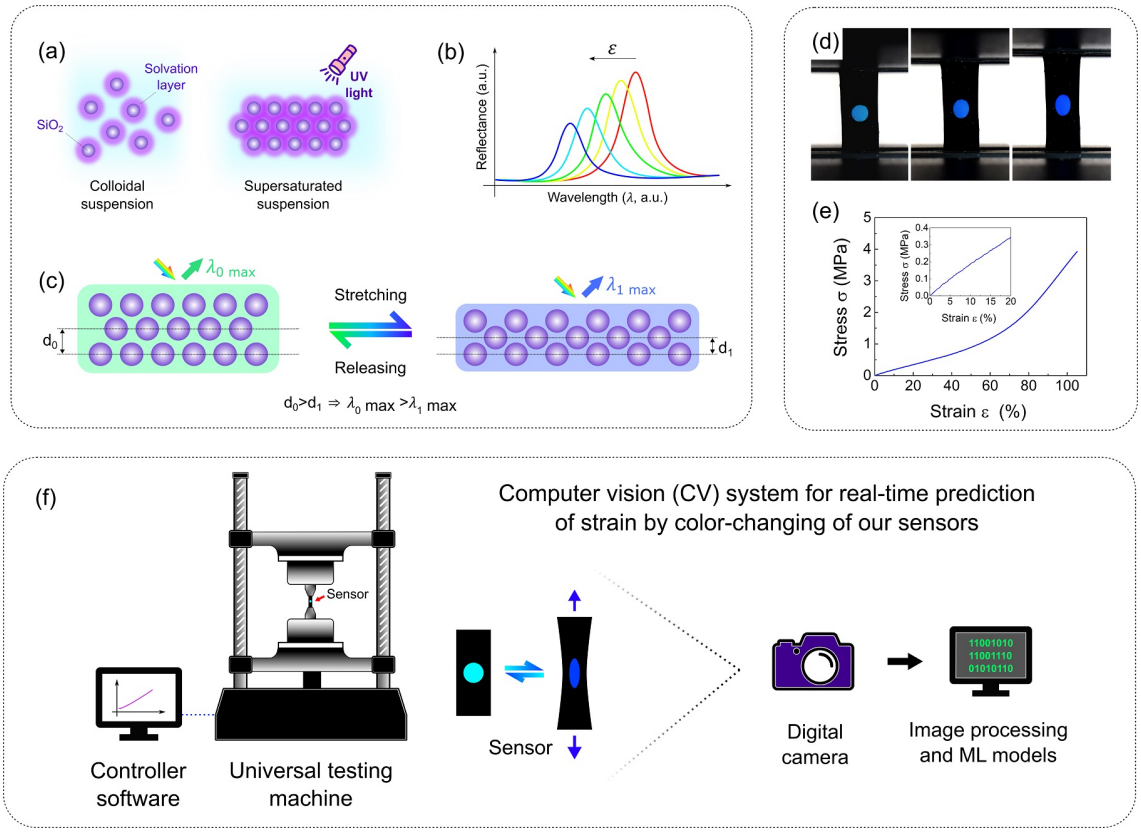

Figure 1. Principles of strain quantification through visual sensing. (a) Scheme of the preparation of the mechanoresponsive core. (b) Strain-induced blueshift of the reflectance spectrum of mechanochromic PC-based materials. (c) Scheme of the reversible changes of structural color during stretching and releasing cycles. (d) From left to right: pictures of mechanochromic strain sensors subjected to ε = 0%; 10%; and 20%, respectively. (e) Stress-strain curve of the mechanochromic strain sensor typical of an elastic behavior at low strain values. (f) Schematic illustration of the computer vision system for real-time prediction of strain by the strain-induced color-changing mechanism in mechanochromic sensors.

To develop the CV system for real-time prediction of strain, 5 mechanochromic sensors were subjected to a series of calibration tensile tests at well-defined strain values where $\varepsilon \in \{0, 2, 4, 6, 8, 10, 12, 14, 16, 18, 20\}$. Pictures of each discrete strain level were taken with an ordinary digital camera and preprocessed before their application in the machine learning models. The pipeline to process the images and predict deformation is illustrated in **Figure 2**. The digital images were converted from the standard RGB to HSV color-space because the latter is more robust to changes in lighting while analyzing color variations across the image. Then, the pictures were preprocessed using well-known techniques to detect only the mechanoresponsive core and image descriptors were extracted from the segmented regions. For further details the reader may refer to the open-source repository at **https://github.com/scabini/mechanosensors**, which allows one to run the pipeline from a set of images. The HSV descriptors can be considered as lower-dimensional representations of the images and were used as input data to the machine learning model. In principle, $\varepsilon \in \mathbb{R}$ can assume any real value between $[0, \infty[$ and dictates the

color-changing feature of the sensors according to **Eq. 1.** Thus, a natural approach would be to consider the relation between strain and reflected structural color as a linear regression problem. Data is constrained to a set of integer labels {0, ..., 20}, which is a limitation of the manual nature of the image acquisition and labeling procedure. However, a fine-tuned linear regression model can learn the linear color transition mechanism and infer any real-valued strain. In this study, we employed 3 regression models: a linear model fitted by minimizing a regularized empirical loss with Stochastic Gradient Descent (SGD), a Ridge regression model(Hoerl & Kennard, 1970), and ElasticNet(Zou & Hastie, 2005). The regression models were evaluated by the coefficient of determination of the prediction (R^2) under both validation strategies. R^2 assesses how strong is the linear relationship between the prediction and the real strain applied on the sensor. Its values range from $]-\infty, 1.0]$, with 1 meaning the best possible score, and 0 representing a model with constant output. The regression results are shown in **Table 1,** with all models performing well. The small difference between the two validation strategies indicates a high robustness of the regression models. The best results are achieved with the Ridge and ElasticNet models, but the latter is slightly more stable during validation with different sensors.

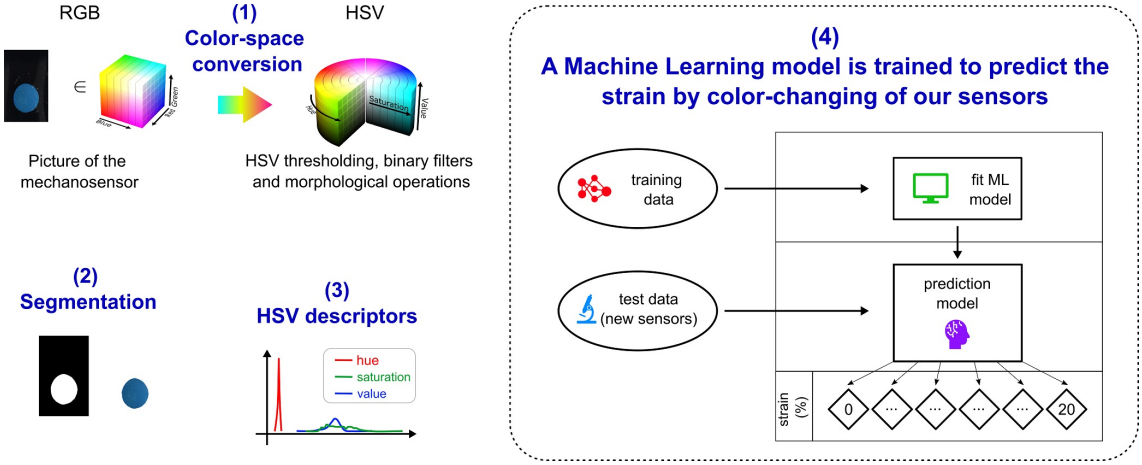

Figure 2. Machine Learning pipeline for automatic measurement of strain through visual information. (1) The input image is first converted to the HSV color-space. *Adapted from https://commons.wikimedia.org/wiki/User:Datumizer licensed under CC BY-SA 3.0 (https://creativecommons.org/licenses/by-sa/3.0/)*. (2) HSV color-space is better suited for segmenting only the region of interest on the sensor. (3) The HSV spectrum of this region is considered to compose image descriptors. (4) Image descriptors are used as input to the machine learning model.

Table 1. Average R^2 for the linear regression models during the task of predicting the real-valued strain from sensor images under different validation strategies.

Validation strategies	SGD	Ridge	ElasticNet
10 repetitions of 5-fold cross validation	0.94 ±0.02	0.98 ±0.01	0.97 ±0.01

Sensor-wise validation	0.89 ±0.09	0.93 ±0.06	0.93 ±0.05

The predictions using the ElasticNet model are less accurate at very low and very high strains, but the dispersion in the values is unlikely to cause mispredictions if averages are considered (**Figure S1**). This shows that the algorithm learned a robust relationship across different strain values in the dataset. Therefore, even though the ElasticNet regression model was exclusively trained with static images constrained to discrete integer classes {0, ..., 20}, the learned linear function should be sufficient to predict intermediate values. Indeed, real-time strain prediction was evaluated using unlabeled videos from tensile tests with the 5 mechanochromic sensors. It is noteworthy that the data from these unlabeled videos were not available to the machine learning algorithm before the analysis. **Figure 3** compares the predicted strain with real values obtained from the controller software of the universal testing machine. A remarkable accuracy is noted with the CV system in the real-time prediction of the applied strain in all mechanochromic sensors, which is demonstrated in the videos in the *Supplementary Material* (**Movies S1 to S5**). The small deviations are attributed to possible differences between the hand-made specimens and illumination variations during the images acquisition process. We are confident that the precision of the algorithm can be further improved by increasing the number of samples during the training stage of the ElasticNet regression model.

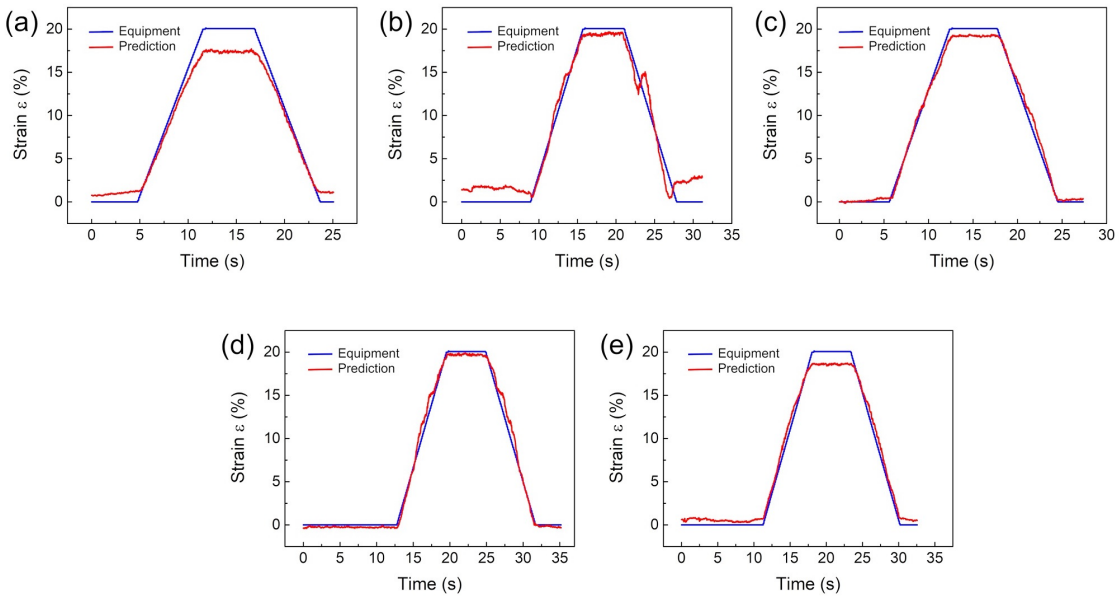

Figure 3. Comparison between the strain prediction of ElasticNet regression model applied on the videos acquired during the tensile test (red line) and the real strain values obtained from the equipment (blue line), for (a-e) sensors 1 to 5, respectively.

An additional feature of the CV platform is the possibility to infer indirectly the tensile force (Load) applied on the mechanochromic sensors. Taking advantage of the near-perfect elastic behavior of the devices at small deformations, a linear function can be adjusted on the strain-load

curves obtained from the data taken during tensile tests (**Figure S2**). **Figure 4** shows that the load can be indirectly estimated by applying the strain prediction values on this function. Therefore, the CV platform is not limited to predicting the strain based on color-changing of the sensors; it can also estimate the tensile force applied. These results point to the next generation of intelligent systems that enables *in situ* visual quantification of strain and tensile forces in a flexible, rapid, and low-cost manner, widening the range of applications of mechanochromic devices.

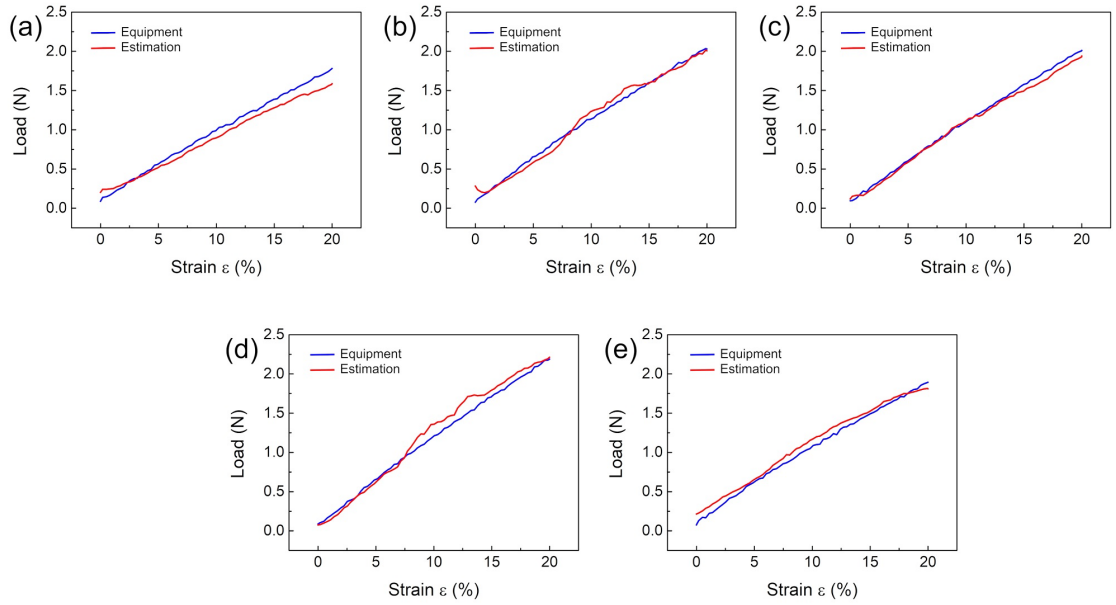

Figure 4. Comparison between the load estimated from the predicted strain (red line) and the real strain-load curves obtained from the equipment during tensile tests (blue line), for (a-e) sensors 1 to 5, respectively.

4. Conclusions

A computer vision (CV) system was developed to predict the strain by the color-changing mechanism of mechanochromic sensors. The relation between strain and reflected structural color was considered as a linear regression problem and Machine Learning algorithms were trained with preprocessed pictures of the sensors subjected to calibration tensile tests. Even though the training data was constrained to a set of integer and discrete strain values, the algorithms could learn a strong linear relation and infer any intermediate real-valued strain. The ElasticNet regression model exhibited the highest precision and stability on the strain prediction task with validation in several sensors (R^2 = 0.93 ±0.05). It had a remarkable performance in predicting real-time strain of sensors during a tensile-relaxion cycle. Due to the near-perfect elastic behavior of the sensors at small deformations, a linear function can be fitted on strain-load data obtained during tensile tests and applied to the predicted strain to estimate the theoretical tensile force applied on the device at each discrete real strain value. It is significant that the high performance was achieved with standard image processing techniques and machine learning algorithms. It is conceivable that more sophisticated applications can be developed in the future

with customized methods. The proposed concept of visual sensing may be used in situations where *in-situ* monitoring of deformation and tensile forces must be done in a noninvasive manner, such as in virtual reality and human-computer interaction systems.

Declaration of Competing Interest

The authors declare that they have no known competing financial interests or personal relationships that could have appeared to influence the work reported in this paper.

Acknowledgments

The authors are grateful to the Department of Materials Engineering (SMM/EESC - USP) for the tensile tests and to NVIDIA GPU Grant Program for the donation of the Quadro P6000 and the Titan Xp GPUs used in this research.

Funding

This research was supported by São Paulo Research Foundation – FAPESP (grants: #2020/02938-0; #2019/07811-0; #2021/07289-2; #2014/08026-1; #2016/18809-9 and #2018/22214-6), INEO, CAPES and CNPq (grant: #307897/2018-4).

References

C de Castro, L. D., & Oliveira, O. N. (2022). Silica Nanoparticle/Polymer Film-Based Soft Mechanochromic Devices for Detecting Mechanical Deformation and Stress Cycles in Varied Environments. *ACS Applied Nano Materials*, *5*(2), 2906–2911. https://doi.org/10.1021/acsanm.2c00102

Chen, Jiayao, Xu, L., Yang, M., Chen, X., Chen, X., & Hong, W. (2019). Highly Stretchable Photonic Crystal Hydrogels for a Sensitive Mechanochromic Sensor and Direct Ink Writing. *Chemistry of Materials*, *31*(21), 8918–8926. https://doi.org/10.1021/acs.chemmater.9b02961

Chen, Jing, Zhang, J., Luo, Z., Zhang, J., Li, L., Su, Y., … Li, H. (2020). Superelastic, Sensitive, and Low Hysteresis Flexible Strain Sensor Based on Wave-Patterned Liquid Metal for Human Activity Monitoring. *ACS Applied Materials & Interfaces*, *12*(19), 22200–22211. https://doi.org/10.1021/acsami.0c04709

Cheng, C.-H., Masuda, S., Nozaki, S., Nagano, C., Hirai, T., Kojio, K., & Takahara, A. (2020). Fabrication and Deformation of Mechanochromic Nanocomposite Elastomers Based on Rubbery and Glassy Block Copolymer-Grafted Silica Nanoparticles. *Macromolecules*, *53*(11), 4541–4551. https://doi.org/10.1021/acs.macromol.9b02031

Dong, Y., Bazrafshan, A., Pokutta, A., Sulejmani, F., Sun, W., Combs, J. D., … Salaita, K. (2019). Chameleon-Inspired Strain-Accommodating Smart Skin. *ACS Nano*, *13*(9), 9918–9926. https://doi.org/10.1021/acsnano.9b04231

Dougherty, E. R., & Lotufo, R. A. (2003). Hands-on Morphological Image Processing. In *Hands-on Morphological Image Processing* (Vol. 25). SPIE. https://doi.org/10.1117/3.501104

Esteva, A., Chou, K., Yeung, S., Naik, N., Madani, A., Mottaghi, A., … Socher, R. (2021). Deep learning-enabled medical computer vision. *Npj Digital Medicine*, *4*(1), 5. https://doi.org/10.1038/s41746-020-00376-2

Gao, W., Ota, H., Kiriya, D., Takei, K., & Javey, A. (2019). Flexible Electronics toward Wearable Sensing [Research-article]. *Accounts of Chemical Research*, *52*(3), 523–533. https://doi.org/10.1021/acs.accounts.8b00500

Gao, Z., Yiu, C., Liu, Y., Li, D., Mei, L., Zeng, Z., & Yu, X. (2020). Stretchable transparent conductive elastomers for skin-integrated electronics. *Journal of Materials Chemistry C*, *8*(43), 15105–15111. https://doi.org/10.1039/D0TC02913K

Hoerl, A. E., & Kennard, R. W. (1970). Ridge Regression: Biased Estimation for Nonorthogonal Problems. *Technometrics*, *12*(1), 55–67. https://doi.org/10.1080/00401706.1970.10488634

Hsieh, C.-H., Lu, Y.-C., & Yang, H. (2020). Self-Assembled Mechanochromic Shape Memory Photonic Crystals by Doctor Blade Coating. *ACS Applied Materials & Interfaces*, *12*(32), 36478–36484. https://doi.org/10.1021/acsami.0c07410

Hu, Y., Wei, B., Yang, D., Ma, D., & Huang, S. (2022). Chameleon-Inspired Brilliant and Sensitive Mechano-Chromic Photonic Skins for Self-Reporting the Strains of Earthworms. *ACS Applied Materials & Interfaces*, *14*(9), 11672–11680. https://doi.org/10.1021/acsami.2c00561

Hu, Y., Yang, D., Ma, D., & Huang, S. (2022). Extremely sensitive mechanochromic photonic crystals with broad tuning range of photonic bandgap and fast responsive speed for high-resolution multicolor display applications. *Chemical Engineering Journal*, *429*, 132342. https://doi.org/10.1016/j.cej.2021.132342

Huang, C., Yao, Y., Montes-García, V., Stoeckel, M., Von Holst, M., Ciesielski, A., & Samorì, P. (2021). Highly Sensitive Strain Sensors Based on Molecules–Gold Nanoparticles Networks for High-Resolution Human Pulse Analysis. *Small*, *17*(8), 2007593. https://doi.org/10.1002/smll.202007593

Karipoth, P., Christou, A., Pullanchiyodan, A., & Dahiya, R. (2022). Bioinspired Inchworm- and Earthworm-like Soft Robots with Intrinsic Strain Sensing. *Advanced Intelligent Systems*, *4*(2), 2100092. https://doi.org/10.1002/aisy.202100092

Kim, J. H., Lee, G. H., Kim, J. Bin, & Kim, S. (2020). Macroporous Hydrogels for Fast and Reversible Switching between Transparent and Structurally Colored States. *Advanced Functional Materials*, *30*(22), 2001318. https://doi.org/10.1002/adfm.202001318

Lee, G. H., Choi, T. M., Kim, B., Han, S. H., Lee, J. M., & Kim, S.-H. (2017). Chameleon-Inspired Mechanochromic Photonic Films Composed of Non-Close-Packed Colloidal Arrays. *ACS Nano*, *11*(11), 11350–11357. https://doi.org/10.1021/acsnano.7b05885

Lee, G. H., Han, S. H., Kim, J. Bin, Kim, J. H., Lee, J. M., & Kim, S.-H. (2019). Colloidal Photonic Inks for Mechanochromic Films and Patterns with Structural Colors of High Saturation [Research-article]. *Chemistry of Materials*, *31*(19), 8154–8162. https://doi.org/10.1021/acs.chemmater.9b02938

Lee, Y., Park, J., Choe, A., Cho, S., Kim, J., & Ko, H. (2020). Mimicking Human and Biological Skins for Multifunctional Skin Electronics. *Advanced Functional Materials*, *30*(20), 1904523. https://doi.org/10.1002/adfm.201904523

Li, M., Tan, H., Jia, L., Zhong, R., Peng, B., Zhou, J., … Zhu, J. (2020). Supramolecular Photonic Elastomers with Brilliant Structural Colors and Broad-Spectrum Responsiveness. *Advanced Functional Materials*, *30*(16), 2000008. https://doi.org/10.1002/adfm.202000008

Li, W., Zhou, Y., Wang, Y., Jiang, L., Ma, J., Chen, S., & Zhou, F. (2021). Core–Sheath Fiber-Based Wearable Strain Sensor with High Stretchability and Sensitivity for Detecting Human Motion. *Advanced Electronic Materials*, *7*(1), 2000865. https://doi.org/10.1002/aelm.202000865

Lin, Y.-H., Siddall, R., Schwab, F., Fukushima, T., Banerjee, H., Baek, Y., … Jusufi, A. (2021). Modeling and Control of a Soft Robotic Fish with Integrated Soft Sensing. *Advanced Intelligent Systems*, *2000244*, 2000244. https://doi.org/10.1002/aisy.202000244

Liu, S., Wang, S., Liu, X., Gandomi, A. H., Daneshmand, M., Muhammad, K., & De Albuquerque, V. H. C. (2021). Human Memory Update Strategy: A Multi-Layer Template Update Mechanism for Remote Visual Monitoring. *IEEE Transactions on Multimedia*, *23*(c), 2188–2198. https://doi.org/10.1109/TMM.2021.3065580

Poloni, E., Rafsanjani, A., Place, V., Ferretti, D., & Studart, A. R. (2022). Stretchable Soft Composites with Strain-Induced Architectured Color. *Advanced Materials*, *34*(6), 2104874. https://doi.org/10.1002/adma.202104874

Qin, M., Li, J., & Song, Y. (2022). Toward High Sensitivity: Perspective on Colorimetric Photonic Crystal Sensors. *Analytical Chemistry*, *94*(27), 9497–9507. https://doi.org/10.1021/acs.analchem.2c01804

Ramadoss, J., Venkatesh, J., Joshi, S., Shukla, P. K., Jamal, S. S., Altuwairiqi, M., & Tiwari, B. (2021). Computer Vision for Human-Computer Interaction Using Noninvasive Technology. *Scientific Programming*, *2021*, 1–15. https://doi.org/10.1155/2021/3902030

Stöber, W., Fink, A., & Bohn, E. (1968). Controlled growth of monodisperse silica spheres in the micron size range. *Journal of Colloid and Interface Science*, *26*(1), 62–69. https://doi.org/10.1016/0021-9797(68)90272-5

Teyssier, J., Saenko, S. V., van der Marel, D., & Milinkovitch, M. C. (2015). Photonic crystals cause active colour change in chameleons. *Nature Communications*, *6*(1), 6368. https://doi.org/10.1038/ncomms7368

Tian, B., Yao, W., Zeng, P., Li, X., Wang, H., Liu, L., … Wu, W. (2019). All-printed, low-cost, tunable sensing range strain sensors based on Ag nanodendrite conductive inks for

wearable electronics. *Journal of Materials Chemistry C*, *7*(4), 809–818. https://doi.org/10.1039/C8TC04753G

Wang, C., Xia, K., Wang, H., Liang, X., Yin, Z., & Zhang, Y. (2019). Advanced Carbon for Flexible and Wearable Electronics. *Advanced Materials*, *31*(9), 1801072. https://doi.org/10.1002/adma.201801072

Wang, Jiangxin, Gao, D., & Lee, P. S. (2021). Recent Progress in Artificial Muscles for Interactive Soft Robotics. *Advanced Materials*, *33*(19), 2003088. https://doi.org/10.1002/adma.202003088

Wang, Jilong, Lu, C., & Zhang, K. (2020). Textile-Based Strain Sensor for Human Motion Detection. *ENERGY & ENVIRONMENTAL MATERIALS*, *3*(1), 80–100. https://doi.org/10.1002/eem2.12041

Wang, L., Liu, W., Yan, Z., Wang, F., & Wang, X. (2021). Stretchable and Shape-Adaptable Triboelectric Nanogenerator Based on Biocompatible Liquid Electrolyte for Biomechanical Energy Harvesting and Wearable Human–Machine Interaction. *Advanced Functional Materials*, *31*(7), 2007221. https://doi.org/10.1002/adfm.202007221

Wang, W., Yang, S., Ding, K., Jiao, L., Yan, J., Zhao, W., … Ni, Y. (2021). Biomaterials- and biostructures Inspired high-performance flexible stretchable strain sensors: A review. *Chemical Engineering Journal*, *425*(April), 129949. https://doi.org/10.1016/j.cej.2021.129949

Wang, Y., Cao, X., Cheng, J., Yao, B., Zhao, Y., Wu, S., … Niu, W. (2021). Cephalopod-Inspired Chromotropic Ionic Skin with Rapid Visual Sensing Capabilities to Multiple Stimuli. *ACS Nano*, *15*(2), 3509–3521. https://doi.org/10.1021/acsnano.1c00181

Wu, W. (2019). Stretchable electronics: functional materials, fabrication strategies and applications. *Science and Technology of Advanced Materials*, *20*(1), 187–224. https://doi.org/10.1080/14686996.2018.1549460

Wu, Y., Wang, Y., Zhang, S., & Wu, S. (2021). Artificial Chameleon Skin with Super-Sensitive Thermal and Mechanochromic Response. *ACS Nano*, *15*(10), 15720–15729. https://doi.org/10.1021/acsnano.1c05612

Yang, J. C., Mun, J., Kwon, S. Y., Park, S., Bao, Z., & Park, S. (2019). Electronic Skin: Recent Progress and Future Prospects for Skin-Attachable Devices for Health Monitoring, Robotics, and Prosthetics. *Advanced Materials*, *31*(48), 1904765. https://doi.org/10.1002/adma.201904765

Yi, H., Lee, S., Ko, H., Lee, D., Bae, W., Kim, T., … Jeong, H. E. (2019). Ultra-Adaptable and Wearable Photonic Skin Based on a Shape-Memory, Responsive Cellulose Derivative. *Advanced Functional Materials*, *29*(34), 1902720. https://doi.org/10.1002/adfm.201902720

Yin, R., Wang, D., Zhao, S., Lou, Z., & Shen, G. (2021). Wearable Sensors-Enabled Human–Machine Interaction Systems: From Design to Application. *Advanced Functional Materials*, *31*(11), 2008936. https://doi.org/10.1002/adfm.202008936

Yuan, J., Chen, C., Yang, W., Liu, M., Xia, J., & Liu, S. (2021). A survey of visual analytics techniques for machine learning. *Computational Visual Media*, *7*(1), 3–36. https://doi.org/10.1007/s41095-020-0191-7

Zhang, Z., Chen, Z., Wang, Y., & Zhao, Y. (2020). Bioinspired conductive cellulose liquid-crystal hydrogels as multifunctional electrical skins. *Proceedings of the National Academy of Sciences*, *117*(31), 18310–18316. https://doi.org/10.1073/pnas.2007032117

Zhao, K., Cao, X., Alsaid, Y., Cheng, J., Wang, Y., Zhao, Y., … Niu, W. (2021). Interactively mechanochromic electronic textile sensor with rapid and durable electrical/optical response for visualized stretchable electronics. *Chemical Engineering Journal*, *426*(May), 130870. https://doi.org/10.1016/j.cej.2021.130870

Zhong, J., Ma, Y., Song, Y., Zhong, Q., Chu, Y., Karakurt, I., … Lin, L. (2019). A Flexible Piezoelectret Actuator/Sensor Patch for Mechanical Human–Machine Interfaces [Research-article]. *ACS Nano*, *13*(6), 7107–7116. https://doi.org/10.1021/acsnano.9b02437

Zou, H., & Hastie, T. (2005). Regularization and Variable Selection via the Elastic Net. *Journal of the Royal Statistical Society. Series B (Statistical Methodology)*, *67*(2), 301–320.